Consistent Hydrodynamics for Phase Field Crystals

V. Heinonen,[1,*] C. V. Achim,[1] J. M. Kosterlitz,[2] See-Chen Ying,[2] J. Lowengrub,[3,4] and T. Ala-Nissila[1,2]

[1]*COMP Centre of Excellence, Department of Applied Physics, Aalto University,*
School of Science, P.O. Box 11100, FI-00076 Aalto, Finland
[2]*Department of Physics, Brown University, Providence, Rhode Island 02912-1843, USA*
[3]*Department of Mathematics, University of California, Irvine, California 92697, USA*
[4]*Department of Chemical Engineering and Materials Science, University of California, Irvine, California 92697, USA*

We use the amplitude expansion in the phase field crystal framework to formulate an approach where the fields describing the microscopic structure of the material are coupled to a hydrodynamic velocity field. The model is shown to reduce to the well-known macroscopic theories in appropriate limits, including compressible Navier-Stokes and wave equations. Moreover, we show that the dynamics proposed allows for long wavelength phonon modes and demonstrate the theory numerically showing that the elastic excitations in the system are relaxed through phonon emission.

One of the grand challenges in materials modeling is to take into account the large range of different time scales from elastic vibrations to vacancy diffusion and length scales varying from atomistic details to dislocations and grain boundaries at micron scales. Phase field crystal (PFC) models were originally introduced [1] in order to couple diffusive time scales with atomistic spatial resolution and are a suitable candidate for a framework with a wide range of temporal scales. This is achieved by coarsening out fluctuations due to finite temperature by describing the system in terms of a mass density field which is averaged over thermal fluctuations. Over the past decade, PFC models have been used successfully to study a wide variety of different phenomena in solids [2].

One of the important advantages of the PFC models is the intrinsic incorporation of elastic energy associated with a fixed interatomic length scale. However, this poses a great challenge for the dynamics of the system: elastic excitations emit phonons which cannot be described using overdamped, purely dissipative dynamics. An attempt to include fast time scales in the dynamics was with the introduction of an explicit second order time derivative in the equation of motion for the PFC mass density field $\tilde{\rho}$ as

$$\partial_t^2 \tilde{\rho} + \alpha \partial_t \tilde{\rho} = \nabla^2 \frac{\delta \tilde{F}}{\delta \tilde{\rho}}, \qquad (1)$$

where $\tilde{F}$ is a PFC free energy and α a dissipation parameter [3,4]. The incorporation of the second order time derivative gives rise to short wavelength oscillations accelerating relaxation processes but fails to describe large scale vibrations. This was pointed out by Majaniemi *et al.* who studied coupling of a displacement field to the mass density field within the PFC framework [5,6].

Fast dynamics have been studied more systematically by coupling a velocity field with the PFC mass density field

[7,8]. However, two main obstacles arise from this sort of coupling. First, the PFC mass density field oscillates at an atomistic length scale creating large gradients which result in spurious unphysical flows. Second, it is not clear how dissipation at microscopic length scales should be incorporated. Hydrodynamics considers smooth fields, and it is hard to extend the theory to spatially microscopic systems with velocity variations at the interatomic length scale.

Some attempts have been made recently to overcome these problems by introducing a mesoscopic mass density which can be obtained by smoothing out the PFC mass density with specific Fourier filters [9] and by considering colloidal systems where hydrodynamics is solved only in the solvent surrounding the colloidal particles [10]. In this Letter, we introduce an approach that avoids the possible ambiguity of coarse graining the fields and that is not limited to colloidal systems.

In this work, we follow the idea of coarse graining the mass density and velocity fields by using the amplitude expansion framework [11,12] where the structure is described by the amplitudes of the atomistic density oscillations instead of the PFC mass density field itself. This framework allows for a description of the material by smooth fields, and it can be shown to reduce to well-known macroscopic theories. The displacement field is naturally coupled to the amplitudes of the density oscillations and to the velocity field, with no need for additional assumptions.

We derive the dynamical equations for the system by first writing down energy conserving dynamics for the PFC system and then coarse graining these equations as well as the energy in order to obtain conserved dynamics for the mesoscopic system generated by a mesoscopic energy. After this, we add dissipation in the system to make the dynamics irreversible. We consider some limits of the model and study the grain rotation problem to make a

connection with relaxing elastic excitations through phonon emission.

Conserved dynamics and coarse graining.—We start by writing down conserved dynamics generated by an effective Hamiltonian

$$\tilde{\mathcal{H}}[\tilde{\rho}, \tilde{\mathbf{v}}] = T[\tilde{\rho}, \tilde{\mathbf{v}}] + \tilde{F}[\tilde{\rho}], \tag{2}$$

where $T[\tilde{\rho}, \tilde{\mathbf{v}}] = \int d\mathbf{r}(\tilde{\rho}|\tilde{\mathbf{v}}|^2/2)$ is the kinetic energy and $\tilde{F}[\tilde{\rho}]$ is any configuration free energy of the PFC type with a periodic ground state in the solid phase. Here, $\tilde{\rho}$, $\tilde{\mathbf{v}}$ are the PFC mass density and velocity fields, respectively. We assume conservation of mass and momentum density given by

$$\partial_t \tilde{\rho} = -\nabla \cdot (\tilde{\rho}\,\tilde{\mathbf{v}}), \tag{3}$$

$$\partial_t (\tilde{\rho}\,\tilde{\mathbf{v}}) = -\nabla \cdot (\tilde{\rho}\,\tilde{\mathbf{v}} \otimes \tilde{\mathbf{v}}) + \tilde{\mathbf{f}}, \tag{4}$$

where $\tilde{\mathbf{f}}$ is a force term determined by total energy conservation.

We expand the density $\tilde{\rho}$ in Fourier space as

$$\tilde{\rho}(\mathbf{r}, t) \approx \rho(\mathbf{r}, t) + \sum_j [\eta_j(\mathbf{r}, t)e^{i\mathbf{q}_j \cdot \mathbf{r}} + \text{c.c.}]. \tag{5}$$

Here, $\mathbf{q}_j$ are the reciprocal lattice vectors, η_j are the amplitudes, ρ is the density field averaged over a unit cell of the Bravais lattice, and c.c. denotes the complex conjugate.

The amplitudes η_j and the density ρ are assumed to be slowly varying in space and are treated as constants over a length scale $1/|\mathbf{q}_j|$. Furthermore, the amplitudes η_j are taken to be complex valued to allow for displacements. Change of coordinates $\mathbf{r} \to \mathbf{r} - \mathbf{u}(\mathbf{r})$ in Eq. (5), where $\mathbf{u}$ is a *spatially slowly varying* displacement field, results in $\eta_j \to \eta_j \exp(-i\mathbf{q}_j \cdot \mathbf{u})$ giving a meaning to the phase of the complex amplitudes.

Following Ref. [12], we coarse grain Eqs. (3) and (4) to obtain time-evolution equations for fields η_j, ρ and a mesoscopic velocity $\mathbf{v}$. We present the results here, the details may be found in the Supplemental Material [13].

From the mass density conservation (3), we get

$$\partial_t \rho = -\nabla \cdot (\rho \mathbf{v}), \tag{6}$$

$$\partial_t \eta_j = -\mathcal{Q}_j \cdot (\eta_j \mathbf{v}), \tag{7}$$

where $\mathcal{Q}_j = \nabla + i\mathbf{q}_j$. The momentum density conservation of Eq. (4) gives

$$\rho\frac{D\mathbf{v}}{Dt} := \rho(\partial_t \mathbf{v} + \mathbf{v} \cdot \nabla \mathbf{v}) = \mathbf{f}, \tag{8}$$

for the mesoscopic velocity with the help of Eq. (6).

The mesoscopic force term $\mathbf{f}$ in Eq. (8) is determined by the conservation of the effective Hamiltonian $\mathcal{H} = T[\rho, \mathbf{v}] + F[\rho, \{\eta_j\}]$, where T is the kinetic energy

$$T = \int d\mathbf{r}\left(\frac{1}{2}\rho|\mathbf{v}|^2\right) \tag{9}$$

and F is a configuration free energy obtained from coarse graining $\tilde{F}$ and described in terms of ρ and $\{\eta_j\}$. We require that $\partial_t \mathcal{H} = 0$. This results in

$$\mathbf{f} = -\rho\nabla\frac{\delta F}{\delta\rho} - \sum_j \left[\eta_j^* \mathcal{Q}_j \frac{\delta F}{\delta\eta_j^*} + \text{c.c.}\right]. \tag{10}$$

For the remainder of this Letter, we choose a configuration free energy of a 2D hexagonal lattice

$$F = \int d\mathbf{r}\Bigg[\frac{B^\ell}{2}\rho^2 - \frac{\tau}{3}\rho^3 + \frac{\nu}{4}\rho^4 + \frac{\tilde{B}^x}{2}|\nabla\rho|^2$$
$$+ \left(\frac{\Delta B}{2} - \tau\rho + \frac{3\nu}{2}\rho^2\right)A^2 + \sum_{j=1}^{3} B^x |\mathcal{G}_j \eta_j|^2$$
$$+ (6\nu\rho - 2\tau)\left(\prod_{j=1}^{3}\eta_j + \text{c.c.}\right) + \frac{3\nu}{4}\left(A^4 - 2\sum_{j=1}^{3}|\eta_j|^4\right)\Bigg], \tag{11}$$

where $A^2 = 2\sum_j |\eta_j|^2$, $\mathcal{G}_j = \nabla^2 + 2i\mathbf{q}_j \cdot \nabla$, $B^\ell = \Delta B + B^x$, τ and ν are bulk energy parameters, and $\tilde{B}^x$ is a surface energy parameter for the density ρ. We have chosen a representation for the vectors $\mathbf{q}_j$ as $\mathbf{q}_1 = (-\sqrt{3}/2, -1/2)$, $\mathbf{q}_2 = (0, 1)$, and $\mathbf{q}_3 = (\sqrt{3}/2, -1/2)$. This energy can be obtained from the standard PFC free energy

$$\tilde{F} = \int d\mathbf{r}\left[\frac{\Delta B}{2}\tilde{\rho}^2 + \frac{B^x}{2}\tilde{\rho}(1 + \nabla^2)^2\tilde{\rho} - \frac{\tau}{3}\tilde{\rho}^3 + \frac{\nu}{4}\tilde{\rho}^4\right]$$

by coarse graining, as discussed in Ref. [20].

Using the configuration free energy F, the functional derivatives in Eq. (10) become

$$\frac{\delta F}{\delta\eta_j^*} = (\Delta B - 2\tau\rho + 3\nu\rho^2)\eta_j + B^x \mathcal{G}_j^2 \eta_j$$
$$+ (6\nu\rho - 2\tau)\prod_{i\neq j}\eta_i^* + 3\nu(A^2 - |\eta_j|^2)\eta_j \tag{12}$$

and

$$\frac{\delta F}{\delta\rho} = (B^\ell + 3\nu A^2 - \tilde{B}^x\nabla^2)\rho - \tau\rho^2$$
$$- \tau A^2 + \nu\rho^3 + 6\nu(\eta_1\eta_2\eta_3 + \text{c.c.}). \tag{13}$$

Dissipation.—To incorporate irreversible effects in the dynamics, we add dissipation. For the time evolution of the velocity, we choose Navier-Stokes-type dissipation resulting in

$$\rho\frac{D\mathbf{v}}{Dt} = \mathbf{f} + \mu_S\nabla^2\mathbf{v} + (\mu_B - \mu_S)\nabla\nabla\cdot\mathbf{v}, \qquad (14)$$

where μ_S is a surface dissipation parameter and μ_B accounts for bulk dissipation. Source terms in the time evolution of the complex amplitude and density provide additional modes of dissipation:

$$\partial_t\eta_j = -\mathcal{Q}_j\cdot(\eta_j\mathbf{v}) - \mu_\eta\frac{\delta\mathcal{H}}{\delta\eta^*}, \qquad (15)$$

$$\partial_t\rho = -\nabla\cdot(\rho\mathbf{v}) + \mu_\rho\nabla^2\frac{\delta\mathcal{H}}{\delta\rho}. \qquad (16)$$

Here, μ_η and μ_ρ are dissipation parameters.

Now, we have complete dynamics for the system determined by Eqs. (14)–(16), and it can be shown that the dynamics leads into a nonincreasing effective Hamiltonian $\mathcal{H}$ in time [13]. Next, we will study some important limits of the theory.

Liquid limit.—A liquid is described by setting the complex amplitudes $\eta_j \to 0$. In this limit, the time-evolution equation for the velocity field becomes

$$\rho\frac{D\mathbf{v}}{Dt} = -\nabla\left(\frac{B^\ell}{2}\rho^2 - \frac{2\tau}{3}\rho^3 + \frac{3\nu}{4}\rho^4\right)$$
$$+ \mu_S\nabla^2\mathbf{v} + (\mu_B - \mu_S)\nabla(\nabla\cdot\mathbf{v}), \qquad (17)$$

which is accompanied by Eq. (16). When the density dissipation parameter $\mu_\rho \to 0$, this pair of equations becomes the Navier-Stokes equations for a compressible flow where the pressure $P = (B^\ell/2)\rho^2 - (2\tau/3)\rho^3 + (3\nu/4)\rho^4$ is described in terms of a virial expansion in ρ. Here, we take the long wavelength limit and discard any derivatives of ρ of higher order than 2. This also removes the dissipation in Eq. (16).

Overdamped limit.—In the limit where μ_η and μ_ρ are large, the set of equations reduces into the usual over-damped amplitude expansion model [20] described by

$$\partial_t\eta_j = -\mu_\eta\frac{\delta F}{\delta\eta_j^*}, \qquad (18)$$

$$\partial_t\rho = \mu_\rho\nabla^2\frac{\delta F}{\delta\rho}. \qquad (19)$$

This limit is achieved also when the dissipation of the velocity is large [13].

Small displacement limit.—Another interesting limit is the limit of small displacements. Writing the complex amplitudes as $\eta_j = \phi_j\exp(-i\mathbf{q}_j\cdot\mathbf{u})$, we can rewrite the system in terms of the order parameter fields ϕ_j and the displacement field $\mathbf{u}$. Assuming a perfect hexagonal crystal implies that $\phi_j = \phi$. Now, Eq. (15) gives

$$\partial_t\phi = -\nabla\cdot(\phi\mathbf{v}) - \frac{1}{2}\mu_\eta\frac{\delta F}{\delta\phi}, \qquad (20)$$

$$\frac{D\mathbf{u}}{Dt} = \mathbf{v} - \frac{1}{2}\mu_\eta\phi^{-2}\frac{\delta F}{\delta\mathbf{u}}, \qquad (21)$$

with the advective derivative $\frac{D}{Dt}$. With small enough displacements $\mathbf{u}$, we assume that ρ and ϕ are constant (ρ_0 and ϕ_0) and keep only $\mathbf{u}$ and $\mathbf{v}$ up to linear order. Furthermore, we assume that $\mathbf{u}$ changes relatively slowly in space discarding all the derivatives of order higher than 2. We obtain

$$\rho_0\partial_t\mathbf{v} = \mathbf{f} \approx -\frac{\delta F}{\delta\mathbf{u}}, \qquad (22)$$

$$\partial_t\mathbf{u} = \mathbf{v} - \frac{1}{2}\mu_\eta\phi^{-2}\frac{\delta F}{\delta\mathbf{u}}, \qquad (23)$$

$$\frac{\delta F}{\delta\mathbf{u}} \approx -3B^x\phi_0^2(\nabla^2\mathbf{u} + 2\nabla\nabla\cdot\mathbf{u}). \qquad (24)$$

Here, we assume that there is no dissipation of velocity. Differentiating Eq. (23) yields

$$\partial_t^2\mathbf{u} = 3B^x\phi_0^2\rho_0^{-1}(\nabla^2\mathbf{u} + 2\nabla\nabla\cdot\mathbf{u})$$
$$+ B^x\mu_\eta\partial_t(\nabla^2\mathbf{u} + 2\nabla\nabla\cdot\mathbf{u}), \qquad (25)$$

by substituting $\partial_t\mathbf{v}$ from Eq. (22) giving us a damped wave equation for the hexagonal crystal symmetry.

With the ansatz $\mathbf{u} = \exp(i\mathbf{k}\cdot\mathbf{r} - \omega t)$, we find the dispersion relation $\omega = \omega(\mathbf{k})$. In particular, for the transverse modes $\mathbf{u} = \mathbf{u}_\perp$ with $\mathbf{k}\cdot\mathbf{u}_\perp = 0$, we obtain

$$\omega_\perp^2 - B^x k^2\mu_\eta\omega_\perp + 3B^x\phi_0^2 k^2\rho_0^{-1} = 0, \qquad (26)$$

which we can solve for $\omega_\perp = \omega_\perp^d + i\omega_\perp^o$ giving

$$\omega_\perp^d = \frac{1}{2}B^x\mu_\eta k^2,$$
$$\omega_\perp^o = \pm\frac{k}{2}\sqrt{\frac{B^x}{\rho_0}(12\phi_0^2 - B^x\mu_\eta^2\rho_0 k^2)}, \qquad (27)$$

if $k^2 < 12\phi_0^2/(B^x\mu_\eta^2\rho_0)$. Here, $\omega_\perp^d$ is the damping component and $\omega_\perp^o$ is the oscillating component. If $k^2 > 12\phi_0^2/(B^x\mu_\eta^2\rho_0)$, we get pure damping with

$$\omega_\perp^d = \frac{1}{2}B^x\mu_\eta k^2 \pm \frac{k}{2}\sqrt{\frac{B^x}{\rho_0}(B^x\mu_\eta^2\rho_0 k^2 - 12\phi_0^2)}, \qquad (28)$$

where the complete solution is a superposition of these two modes.

Figure 1 shows the dispersion relation for the oscillating component in the damping and oscillating cases. Our result shows that in the long wavelength limit, the oscillating
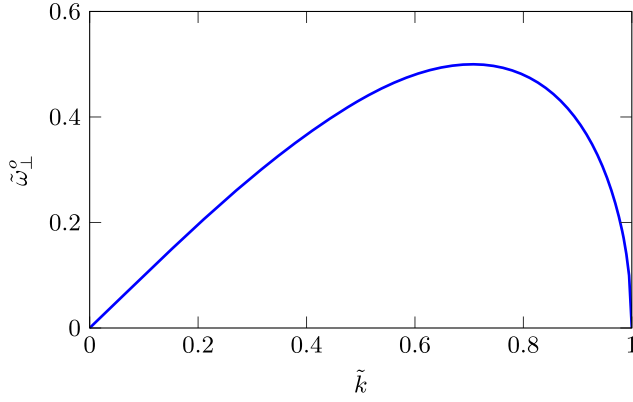
FIG. 1.   The dispersion relation $\tilde{\omega}_{\perp}^{o}(\tilde{k}) = \tilde{k}\sqrt{1-\tilde{k}^2}$ for the oscillating component of the transversal wave in the small displacement limit. Here, $\tilde{\omega}_{\perp}^{o} = \omega_{\perp}^{o}\rho_0\mu_\eta/(6\phi_0^2)$ and $\tilde{k}^2 = k^2 B^x \mu_\eta^2 \rho_0/(12\phi_0^2)$. See the text for details.

small displacement modes correspond to propagating phonons. For wavelengths below a critical value, the modes become purely diffusive. This is in contrast to previous studies [3,4] using Eq. (1), where only diffusive modes exist in the long wavelength limit [6]. Note that when $\mu_\eta = 0$, the damping vanishes, resulting in an energy conserving wave equation with longitudinal and transverse modes with velocities $c_t^2 = 3B^x\phi_0^2\rho_0^{-1}$ for transverse and $c_l^2 = 9B^x\phi_0^2\rho_0^{-1}$ for longitudinal modes.

   Grain rotation.—To test the theory numerically, we study the dynamics of a rotated circular crystalline grain embedded in a crystalline matrix. Although experimental studies of polycrystalline patterns suggest that smaller grains usually disappear at the boundary of two larger grains rather than in the middle of a single matrix [21], the rotated grain remains important for understanding grain boundary motion and has been studied theoretically [22] using molecular dynamics simulations [23,24] and PFC models [25,26].

   The initial misorientation gives rise to a grain boundary at the perimeter of the grain due to a difference in the orientation of the crystal with respect to the surrounding matrix. Taken that the grain boundary motion is curvature driven, it is expected that the area of the grain decreases linearly in time as the rotation angle increases [26]. The increase of the rotation angle is due to the conservation of dislocation cores whose number is proportional to $\gamma(t)R(t)$, where γ is the misorientation angle and R is the radius of the grain. In our calculations, we fixed the energy parameters and varied the velocity dissipation parameter μ_S keeping it equal to μ_B.

   Figure 2 shows the density field ρ and the velocity field **v** during the shrinking process exposing the dislocation cores at the boundary of the grain and showing the rotation of the grain facilitated by the velocity field **v**. Note that the slowly varying density ρ does not vary much even at dislocation cores.
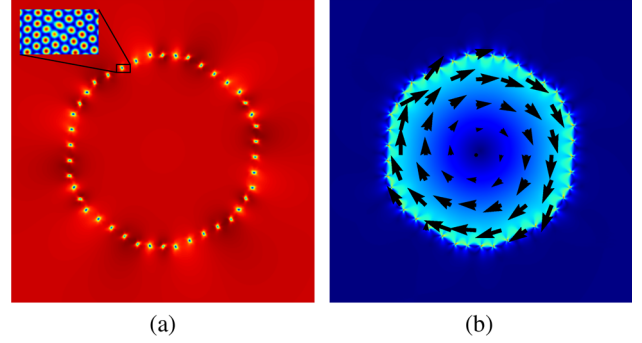
FIG. 2.   (a) The density field ρ with a blowup of the reconstructed PFC density field $\tilde{\rho}$. (b) The magnitude of the velocity field $|\mathbf{v}|$ with a quiver field on top to show the direction of **v**.

   The rate of shrinking is shown in Fig. 3. The shrinking of the grain and also the energy dissipation are faster when we decrease the dissipation parameter μ_S. For comparison, we have included a calculation with overdamped dynamics given by Eqs. (18) and (19) and also overdamped dynamics with elastic equilibration, where the energy is minimized with respect to the deformation field **u** at all times as described in Ref. [27]. The calculations verify the analytical analysis, in particular, that R^2 decreases linearly in time and that the value of γR remains the same regardless of the dynamics.

   Changing μ_S changes the rate of the dynamics. The dynamics in the $\mu_S \to 0$ limit is very similar to dynamics subject to the constraint of elastic equilibrium, and we suspect the fast dynamics when $\mu_S \to 0$ is caused by the minimization of elastic excitations by creation of vibrations which are present throughout the shrinking process with hydrodynamics. We keep ρ constant for overdamped dynamics with and without elastic equilibration since the effect of density is negligible in the absence of hydrodynamics. The initial configuration was identical for all the different cases with a misorientation angle of 5° and a grain diameter half of the domain width. For numerical details, see Ref. [28].
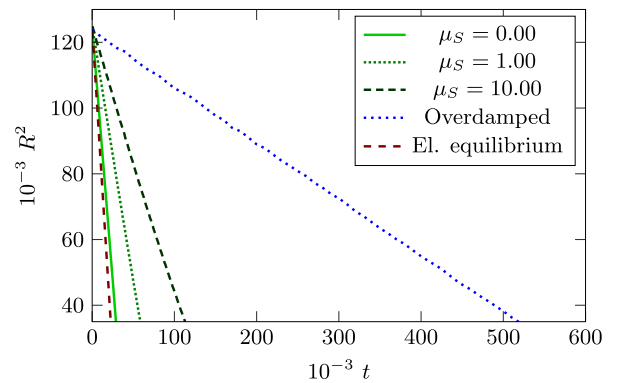
FIG. 3.   The squared radius R^2 of the grain as a function of time for various different values of μ_S and for overdamped dynamics and elastically equilibrated overdamped dynamics.

Summary and discussion.—We introduce a scheme which couples fast dynamics to dissipative processes on a mesoscopic length scale. The dynamics arises from conservation laws which couple a velocity field with the fields describing the structure of the system in a consistent manner. We have also shown with a numerical example how the dynamics changes due to the presence of vibrating modes.

The method presented here allows for different types of dissipation in the time evolution of the system. For example, instead of the Navier-Stokes-type dissipation used here, one could use a Langevin-type dissipation $-\mu_L \mathbf{v}$ in the velocity equation (14). This breaks the Galilean invariance of the velocity equation and introduces dissipation similar to that commonly used in PFC dynamics as shown by linearizing hydrodynamics [7]. The Navier-Stokes-type dissipation used here avoids the problem of bulk dissipation described in Ref. [26] since the velocity is Galilean invariant, allowing for parallel transport of all fields while the dissipation takes place only when $\nabla^2 \mathbf{v} \neq 0$ so that uniform motion does not dissipate energy. This also suggests that large grains are more sluggish with traditional PFC dynamics described by Eq. (1) than with the full hydrodynamics since dissipation happens everywhere in the grain rather than just at the perimeter.

The approach of this Letter is general and can be extended to any configuration free energy F which can be written in terms of slowly varying complex amplitudes and density field. We expect this approach to be useful for problems where lattice vibrations, mass transport, and other fast phenomena are coupled to the solid-liquid symmetry breaking. Some examples of such problems are fracture dynamics, fast solidification, and coarsening of polycrystalline patterns.

*vili.heinonen@aalto.fi

[1] K. R. Elder, M. Katakowski, M. Haataja, and M. Grant, Phys. Rev. Lett. **88**, 245701 (2002).

[2] H. Emmerich, H. Löwen, R. Wittkowski, T. Gruhn, G. I. Tóth, G. Tegze, and L. Gránásy, Adv. Phys. **61**, 665 (2012).

[3] P. Stefanovic, M. Haataja, and N. Provatas, Phys. Rev. Lett. **96**, 225504 (2006).

[4] P. Galenko, D. Danilov, and V. Lebedev, Phys. Rev. E **79**, 051110 (2009).

[5] S. Majaniemi and M. Grant, Phys. Rev. B **75**, 054301 (2007).

[6] S. Majaniemi, M. Nonomura, and M. Grant, Eur. Phys. J. B **66**, 329 (2008).

[7] J. A. P. Ramos, E. Granato, S. C. Ying, C. V. Achim, K. R. Elder, and T. Ala-Nissila, Phys. Rev. E **81**, 011121 (2010).

[8] A. Baskaran, A. Baskaran, and J. Lowengrub, J. Chem. Phys. **141**, 174506 (2014).

[9] G. I. Tóth, L. Gránásy, and G. Tegze, J. Phys. Condens. Matter **26**, 055001 (2014).

[10] S. Praetorius and A. Voigt, J. Chem. Phys. **142**, 154904 (2015).

[11] N. Goldenfeld, B. P. Athreya, and J. A. Dantzig, Phys. Rev. E **72**, 020601 (2005).

[12] B. P. Athreya, N. Goldenfeld, and J. A. Dantzig, Phys. Rev. E **74**, 011601 (2006).

[13] See Supplemental Material at http://link.aps.org/supplemental/10.1103/PhysRevLett.116.024303, which includes Refs. [14–19], for more information on the derivation of the theory, the limiting cases, and the numerical methods.

[14] G. Tegze, G. Bansel, G. I. Tóth, T. Pusztai, Z. Fan, and L. Gránásy, J. Comput. Phys. **228**, 1612 (2009).

[15] B. P. Vollmayr-Lee, and A. D. Rutenberg, Phys. Rev. E **68**, 066703 (2003).

[16] J. Zhu, L. Q. Chen, J. Shen, and V. Tikare, Phys. Rev. E **60**, 3564 (1999).

[17] NVIDIA Corporation, http://developer.nvidia.com/cuda-zone.

[18] NVIDIA Corporation, https://developer.nvidia.com/cuFFT.

[19] M. Frigo and S. Johnson, Proc. IEEE **93**, 216 (2005).

[20] D.-H. Yeon, Z.-F. Huang, K. R. Elder, and K. Thornton, Philos. Mag. **90**, 237 (2010).

[21] C. Harrison, D. E. Angelescu, M. Trawick, Z. Cheng, D. a. Huse, P. M. Chaikin, D. a. Vega, J. M. Sebastian, R. a. Register, and D. H. Adamson, Europhys. Lett. **67**, 800 (2004).

[22] J. W. Cahn and J. E. Taylor, Acta Mater. **52**, 4887 (2004).

[23] M. Upmanyu, D. Srolovitz, A. Lobkovsky, J. Warren, and W. Carter, Acta Mater. **54**, 1707 (2006).

[24] Z. Trautt and Y. Mishin, Acta Mater. **60**, 2407 (2012).

[25] K.-A. Wu and P. W. Voorhees, Acta Mater. **60**, 407 (2012).

[26] A. Adland, Y. Xu, and A. Karma, Phys. Rev. Lett. **110**, 265504 (2013).

[27] V. Heinonen, C. V. Achim, K. R. Elder, S. Buyukdagli, and T. Ala-Nissila, Phys. Rev. E **89**, 032411 (2014).

[28] The parameters used for the grain rotation calculation are $B^x = \tilde{B}^x = 1$, $\Delta B = 0.097$, $\mu_\rho = 0.05$, $\mu_\eta = 1$, $\tau = 0.885$, $\nu = 1$. For the spatial discretization, we used $\Delta x = \Delta y = 2$ with a numerical grid of 768×768, while for the temporal discretization, we used a forward Euler method with a time step of $\Delta t = 0.125$. For more details, see the Supplemental Material.